Supplementary Material

Symmetrical and unsymmetrical dicopper complexes, based on bis-oxazoline units: synthesis, spectroscopic properties and reactivity

James A. Isaac, Gisèle Gellon, Florian Molton, Christian Philouze, Nicolas Le Poul, Catherine Belle* and Aurore Thibon-Pourret*

Table of Contents

1-Ligand characterizations

1-1.^{1}H and ^{13}C NMR spectra

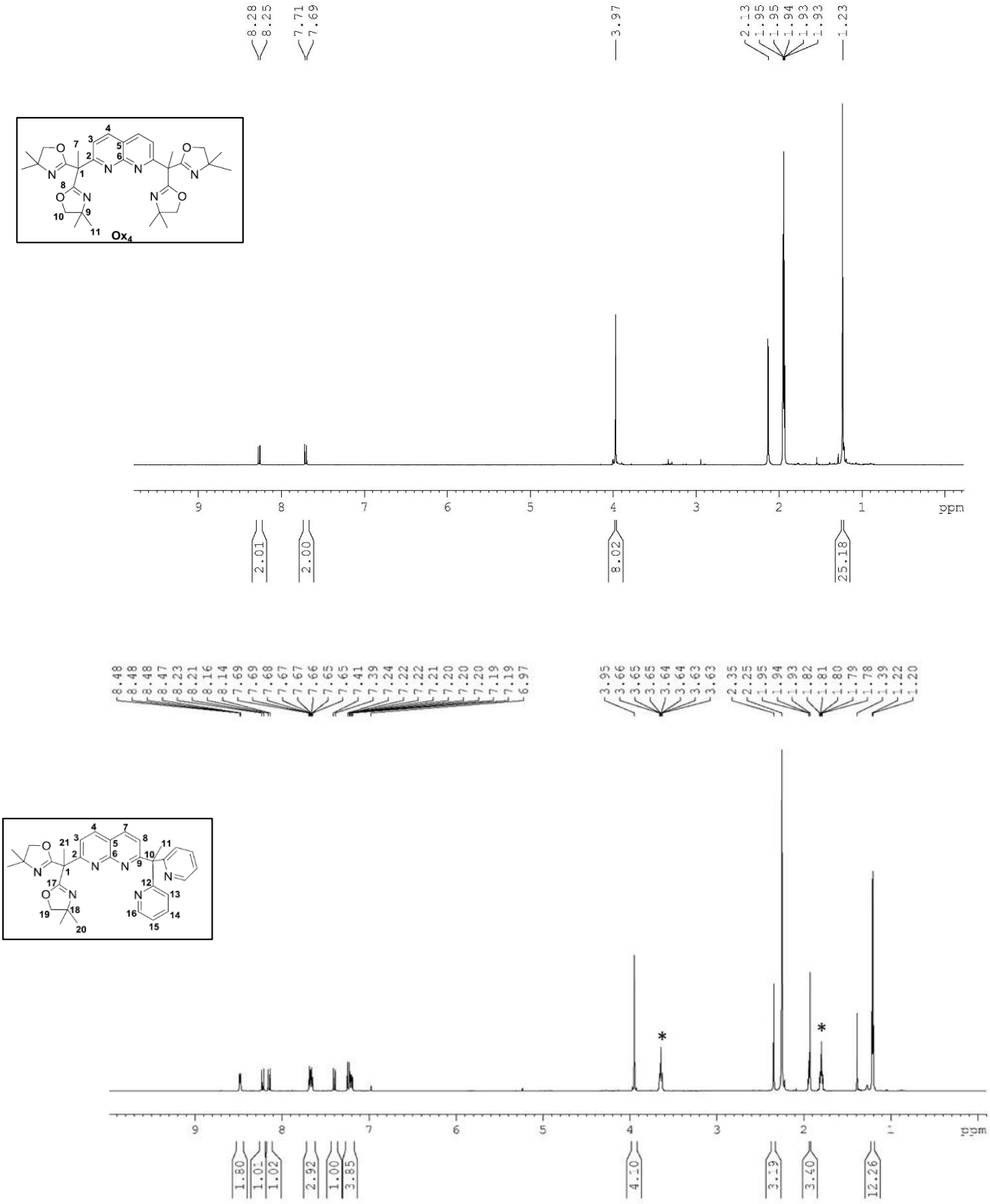

Figure S1: ^{1}H NMR spectra of ligand Ox_4 (top) and Ox_2Py_2 (bottom) in CD_3CN, starred peaks: THF

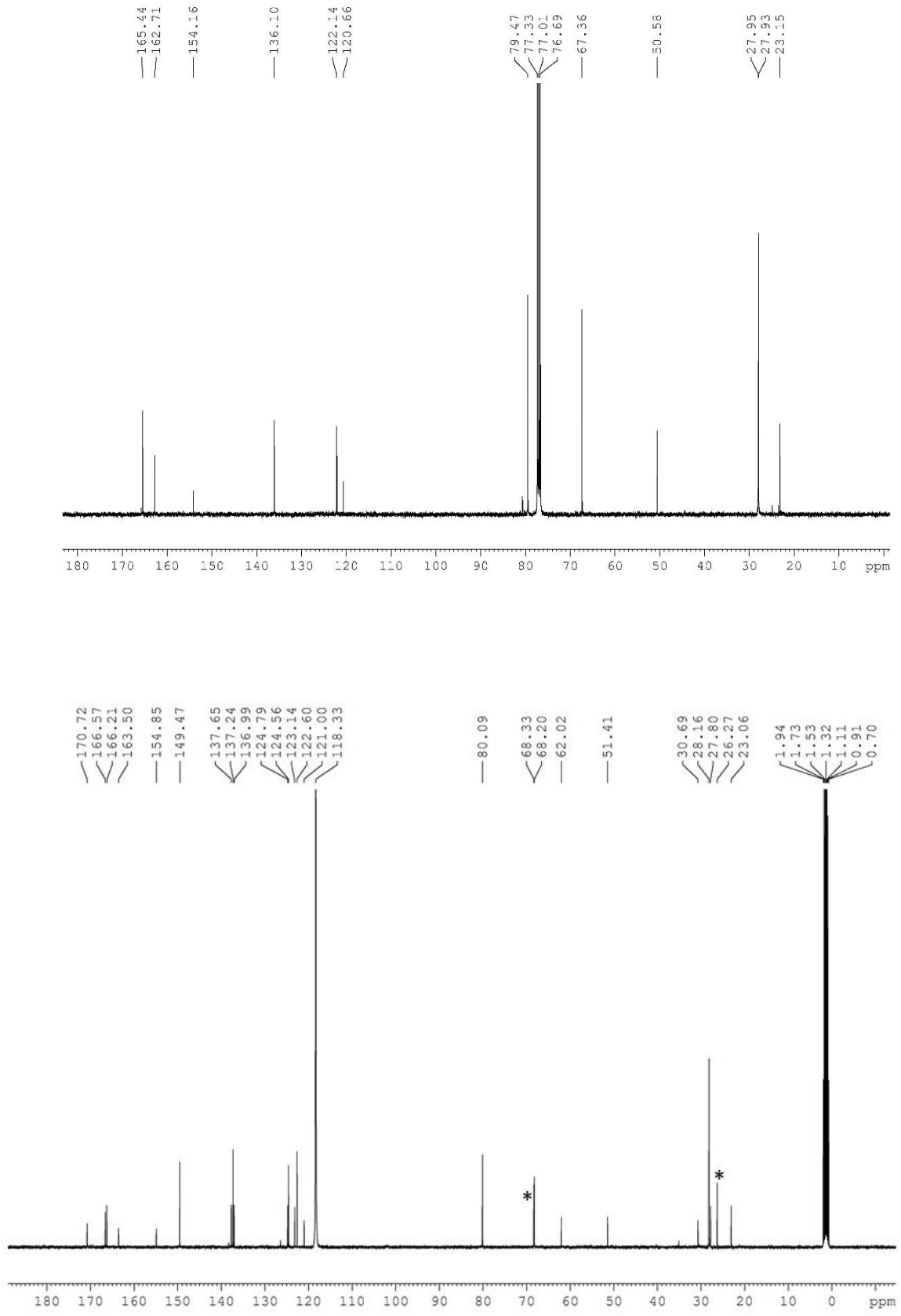

Figure S2: ^{13}C NMR spectra of ligand Ox_4 (top) in $CDCl_3$ and B: Ox_2Py_2 (bottom) in CD_3CN, starred peaks: THF

1-2. ESI-MS spectra

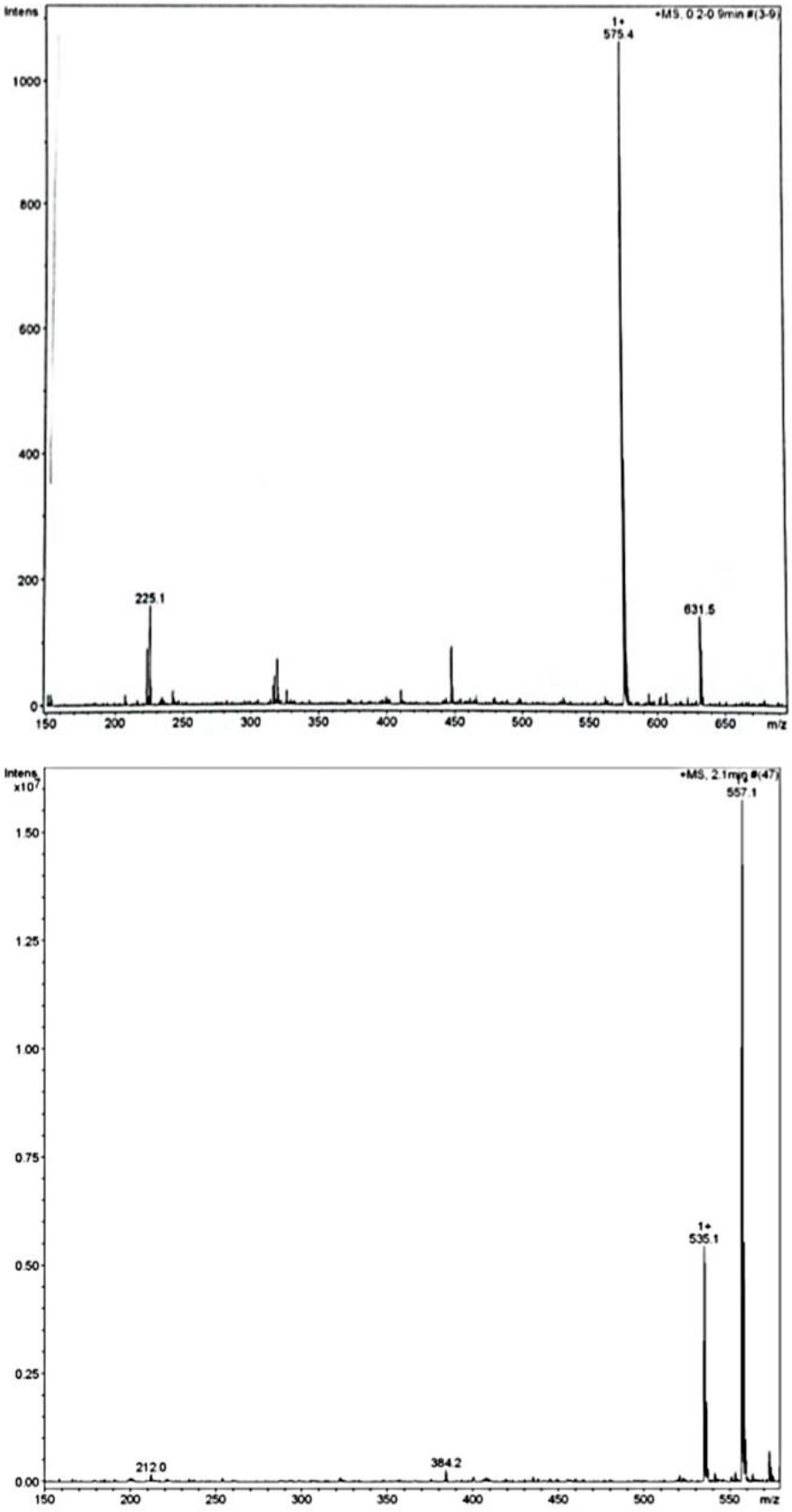

Figure S3: ESI-MS spectra of ligand Ox_4 (top) in CH_2Cl_2 and B: Ox_2Py_2 (bottom) in MeOH, C = 5.10^{-5} M

2-Dicopper(I) complexes characterizations

2-1. ^{1}H NMR

Ligand

Corresponding Cu^{I}_2 complex

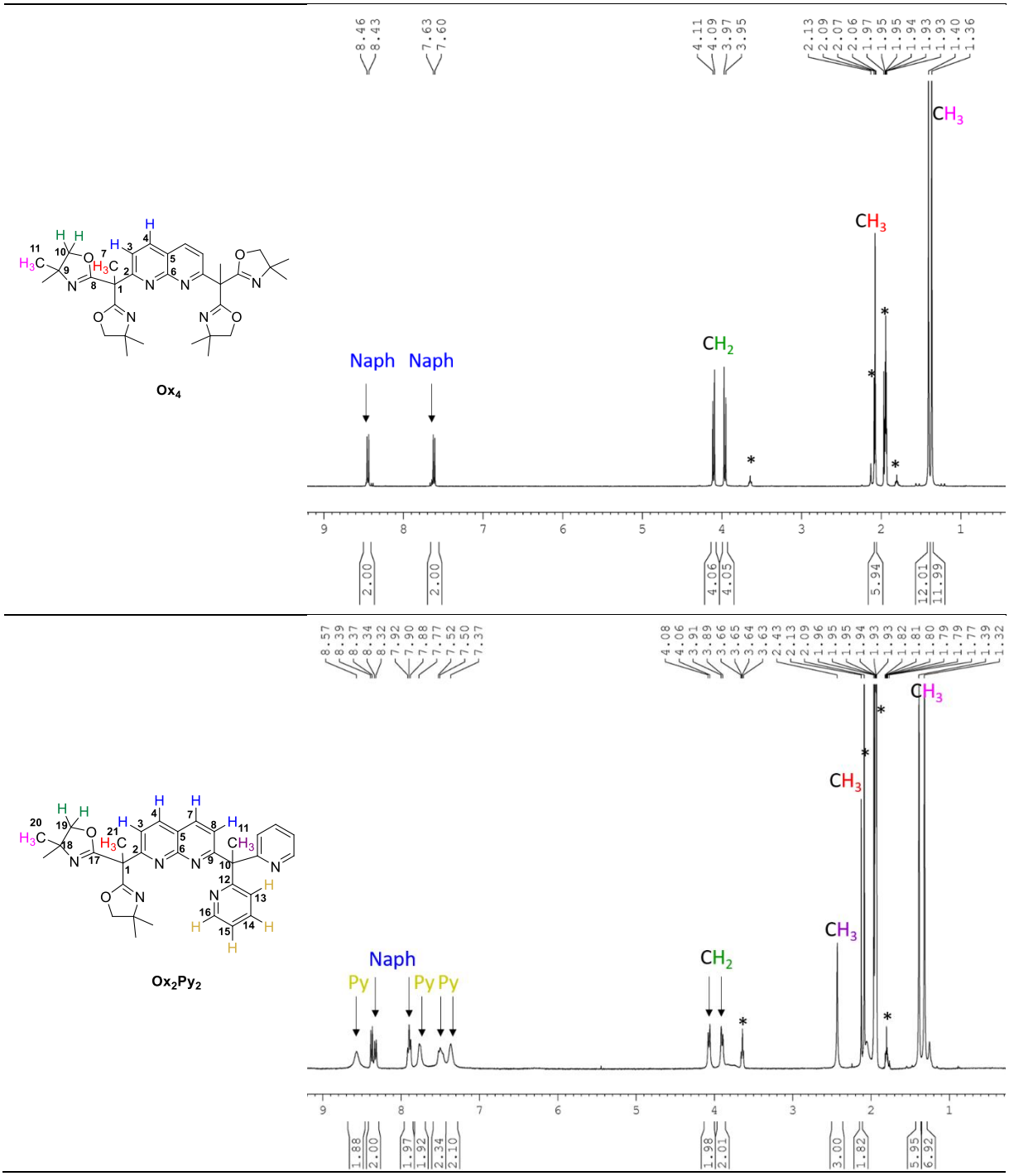

Figure S4: ^{1}H-NMR spectra of $Cu^{I}_2Ox_4$ (top) and $Cu^{I}_2Ox_2Py_2$ (bottom) in CD_3CN, with representations of the relevant ligands (left). Starred peaks from left to right: THF, water, acetonitrile and THF.

3. Reactivity of Cu^{I}_2 complexes

3-1. Reactivity with O_2

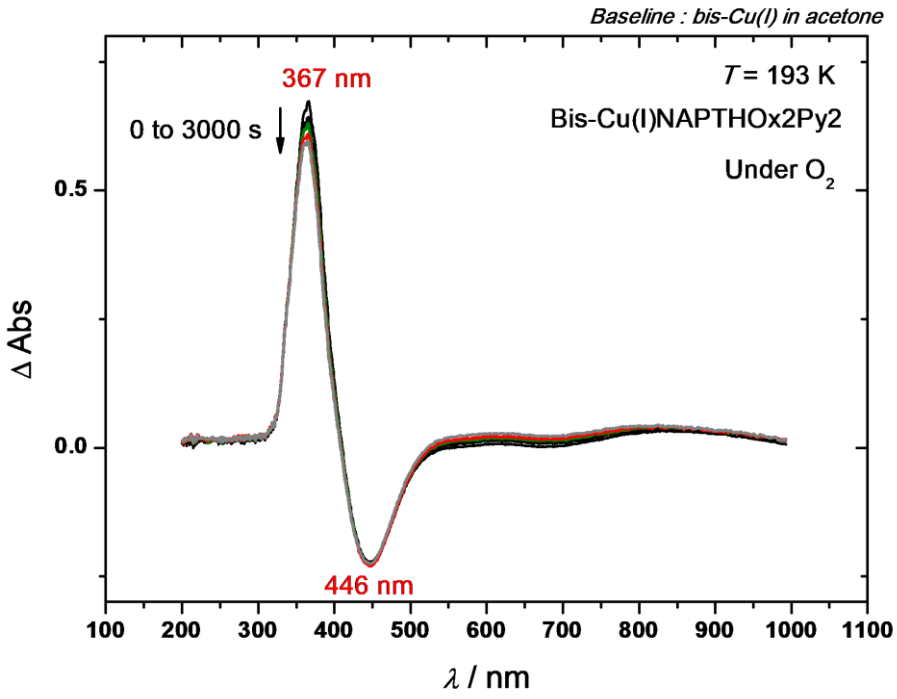

Figure S5: UV-vis spectrum after addition of O_2 to the complex $Cu^{I}_2Ox_2Py_2$. Parameters: optical path = 1 cm; solvent acetone; concentration 0.33 mM, *T* = 193 K. The baseline was taken on the $Cu^{I}_2Ox_2Py_2$ complex in acetone, explaining the use of Δ Abs. instead of Abs. The absorption band at λ = 367 nm is characteristic of the peroxide, thus allowing full the monitoring of its stability at 193 K. The negative value of Δ Abs. at λ = 446 nm corresponds to the disappearance of the MLCT band for the bis-Cu(I) species upon addition of O_2. It remains constant over the experiment duration, showing no back transformation of the peroxide into the bis-Cu(I) species.

3-2: Reactivity of the Cu_2:O_2 species with external substrates.

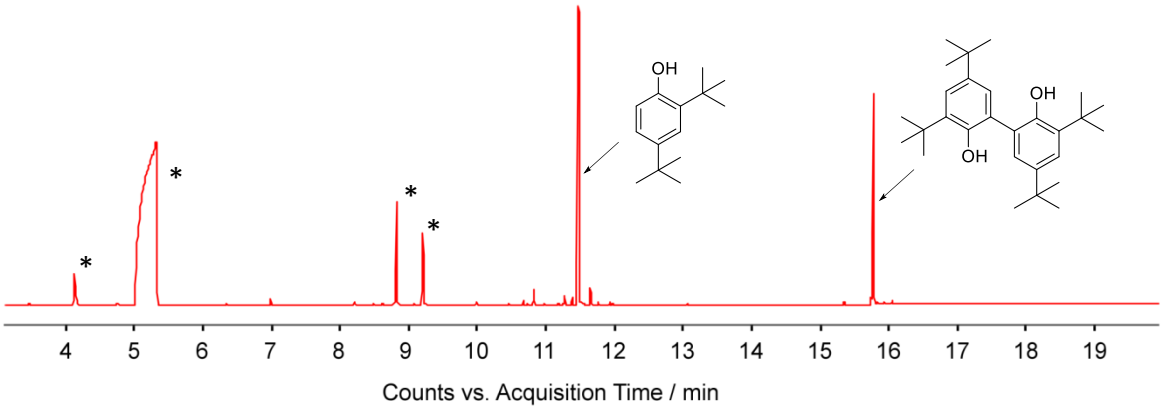

Figure S6: GCMS of the resulting solution after reaction of the μ-η^2:η^2-peroxido-Cu^{II}_2 species from complex $Cu^{I}_2Ox_4$ with 2,4-di-*tert*-butylphenol at 193 K < T < 203 K. Starred peaks are present in the acetone (the solvent used). Results from the complex $Cu^{I}_2Ox_2Py_2$ are very similar.

4- Characterizations of dicopper(II) complexes and mono-oxidized species

4-1. X-Ray diffraction

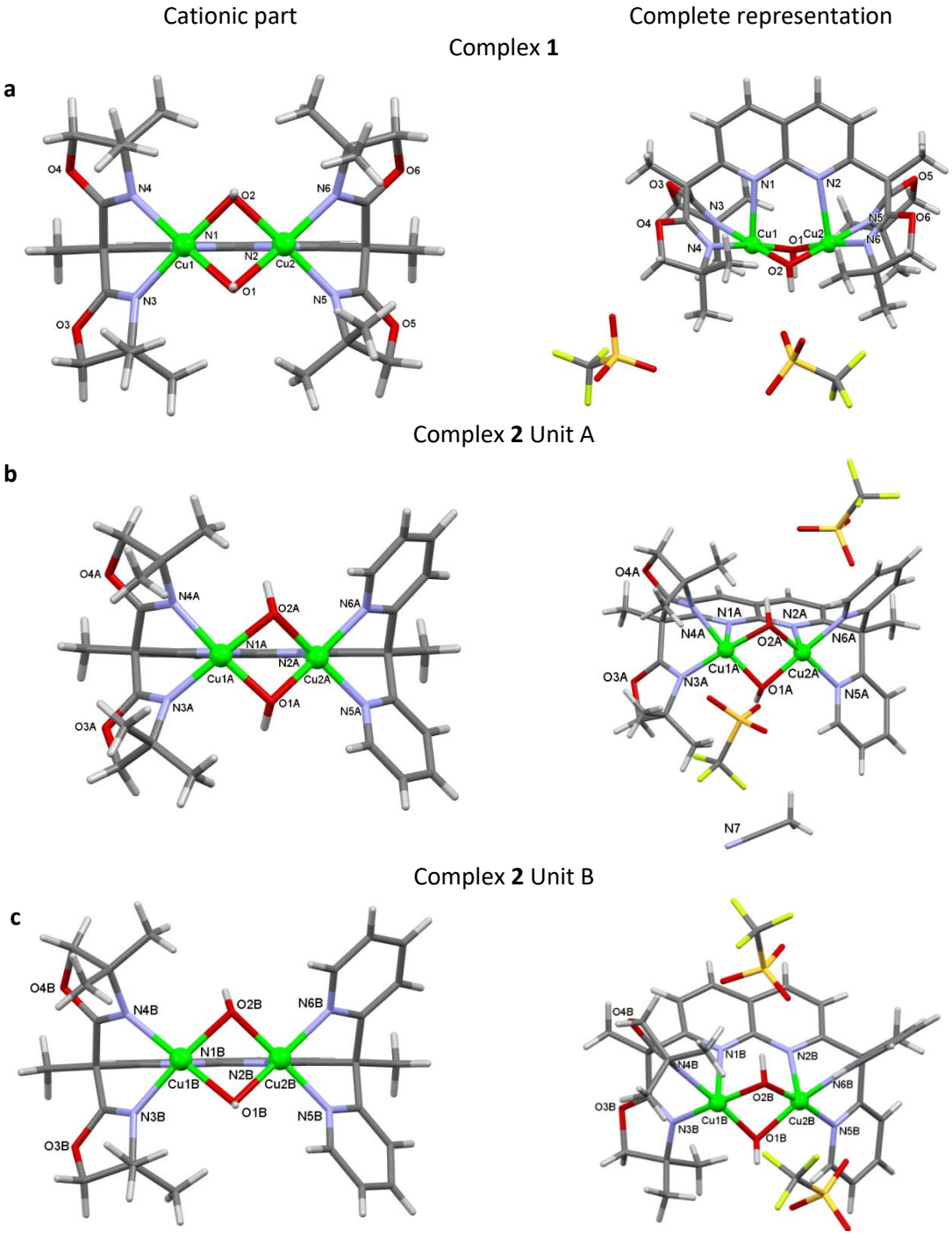

Figure S7: *Left*: View along the plane of the naphthyridine group for cationic part of a) **1**, b) **2A** and c) **2B**
Right: complete representation with the triflate counteranions and solvent of a) **1**, b) **2A** and c) **2B**

Table S1. Selected bond distances [Å] in **1**, **2A** and **2B** from X-ray data.

1	**2A**	**2B**
Cu1···Cu2 2.7537(5)	Cu1A···Cu2A 2.795(1)	Cu1B···Cu2B 2.774(1)
Cu1–O1 1.934(2)	Cu1A–O1A 1.932(4)	Cu1B–O1B 1.949 (5)
Cu1–O2 1.941(2)	Cu1A–O2A 1.938(4)	Cu1B–O2B 1.924(4)
Cu1–N3 2.016(2)	Cu1A–N3A 1.977(5)	Cu1B–N3B 2.004(5)
Cu1–N4 2.010(2)	Cu1A–N4A 2.010(5)	Cu1B–N4B 1.978 (6)
Cu1–N1 2.427(2)	Cu1A–N1A 2.470(5)	Cu1B–N1B 2.482(5)
Cu2–O1 1.940(2)	Cu2A–O1A 1.929(4)	Cu2B–O1B 1.949(5)
Cu2–O2 1.946(2)	Cu2A–O2A 1.940(4)	Cu2B–O2B 1.927(5)
Cu2–N5 1.997(2)	Cu2A–N5A 1.991(5)	Cu2B–N5B 2.000 (7)
Cu2-N6 2.011(2)	Cu2A-N6A 1.996(5)	Cu2B-N6B 1.981(5)
Cu2-N2 2.460(2)	Cu2A-N2A 2.259(5)	Cu2B-N2B 2.288(5)

Table S2. Selected bond angles [°] in **1**, **2A** and **2B** from X-ray data.

1	**2A**	**2B**
O1–Cu2–O2 82.13(7)	O1A–Cu2A–O2A 80.47(18)	O1B–Cu2B–O2B 81.5(2)
O1–Cu1–N4 94.33(7)	O1A–Cu1A–N4A 174.1(2)	O1B–Cu1B–N4B 174.8(2)
O1–Cu2–N6 173.82(7)	O1A–Cu2A–N6A 169.0(2)	O1B–Cu2B–N6B 166.9(2)
O1–Cu1–O2 82.41(6)	O1A–Cu1A–O2A 80.45(18)	O1B–Cu1B–O2B 81.7(2)
O2–Cu1–N4 94.33(7)	O2A–Cu1A–N4A 94.8(2)	O2B–Cu1B–N4B 98.0(2)
O2–Cu2–N6 94.97(7)	O2A–Cu2A–N6A 93.7(2)	O2B–Cu2B–N6B 95.2(2)
O2– Cu2–N2 96.80(6)	O2A– Cu2A–N2A 105.18(19)	O2B– Cu2B–N2B 101.92(19)
N3–Cu1–N4 88.43(7)	N3A–Cu1A–N4A 87.3(2)	N3B–Cu1B–N4B 87.7(2)
N5–Cu2–N6 87.10(8)	N5A–Cu2A–N6A 87.6(2)	N5B–Cu2B–N6B 88.2(2)
O2–Cu1–N4 94.33(7)	O2A–Cu1A–N4A 94.8(2)	O2B–Cu1B–N4B 94.0(2)
O1–Cu2–N5 95.81(7)	O1A–Cu2A–N5A 96.1(2)	O1B–Cu2B–N5B 93.7(2)
Cu1–O1–Cu2 90.39(6)	Cu1A–O1A–Cu2A 92.75(18)	Cu1B–O1B–Cu2B 92.75(18)
Cu1–O2–Cu2 90.39(6)	Cu1A–O2A–Cu2A 92.24(18)	Cu1B–O2B–Cu2B 92.24(18)

4-2. ESI-MS for complexes **1** and **2**

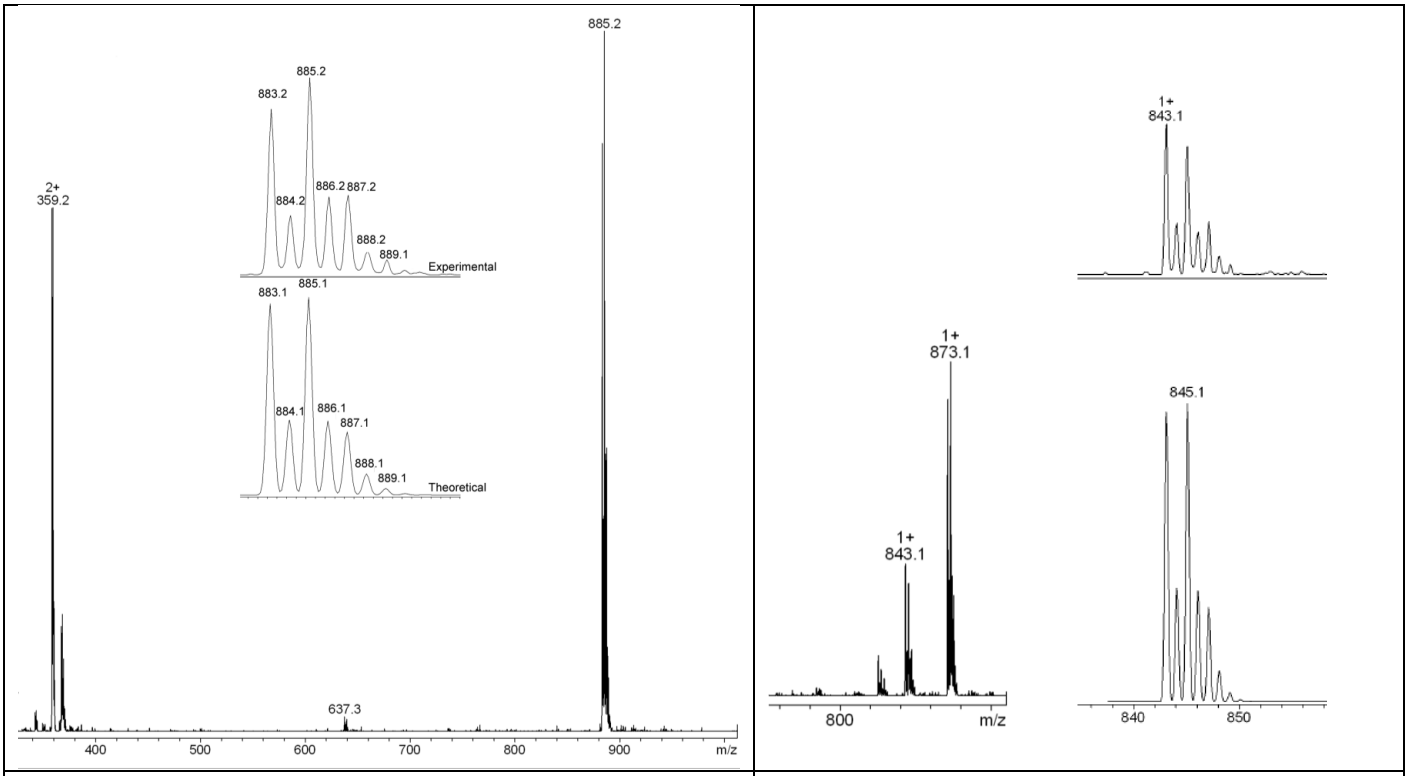

Complex **1** | Complex **2**

Figure S8: ESI-MS spectra of complexes $Cu^{II}_2Ox_4$ (**1**)(left) and $Cu^{II}_2Ox_2Py_2$ (**2**)(right); recorded in acetonitrile. Inset: theoretical and experimental isotopic profiles of the peaks at *m/z* = 883 and 843

4-3. Electrochemical studies

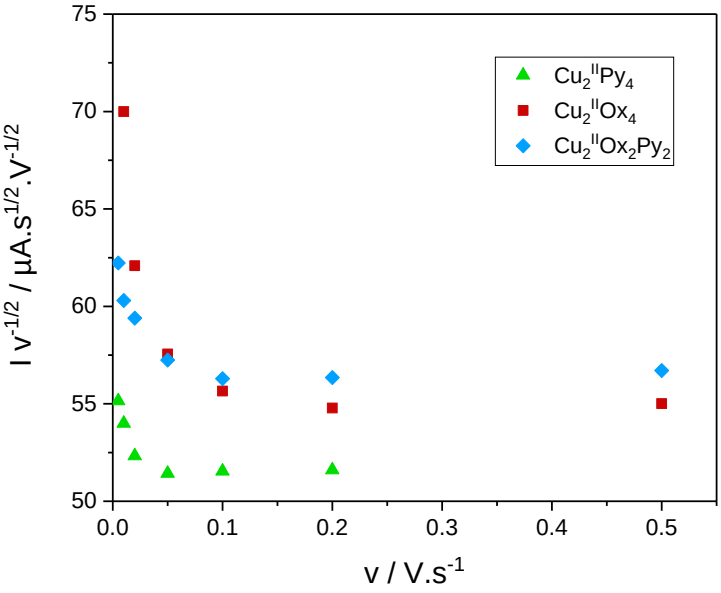

Figure S9: Plots of the normalized peak current $Iv^{-1/2}$ (where *I* is the peak current on the CV) against the scan rate v for complexes **1**, **2** and $[(Cu_2(Py_4))(\mu\text{-}OH)_2](CF_3SO_3)_2$ in concentration of 0.70 mM, 0.68 mM and 0.85 mM respectively in CH_3CN/NBu_4ClO_4 0.1 M at 298 K. Working electrode : glassy carbon.

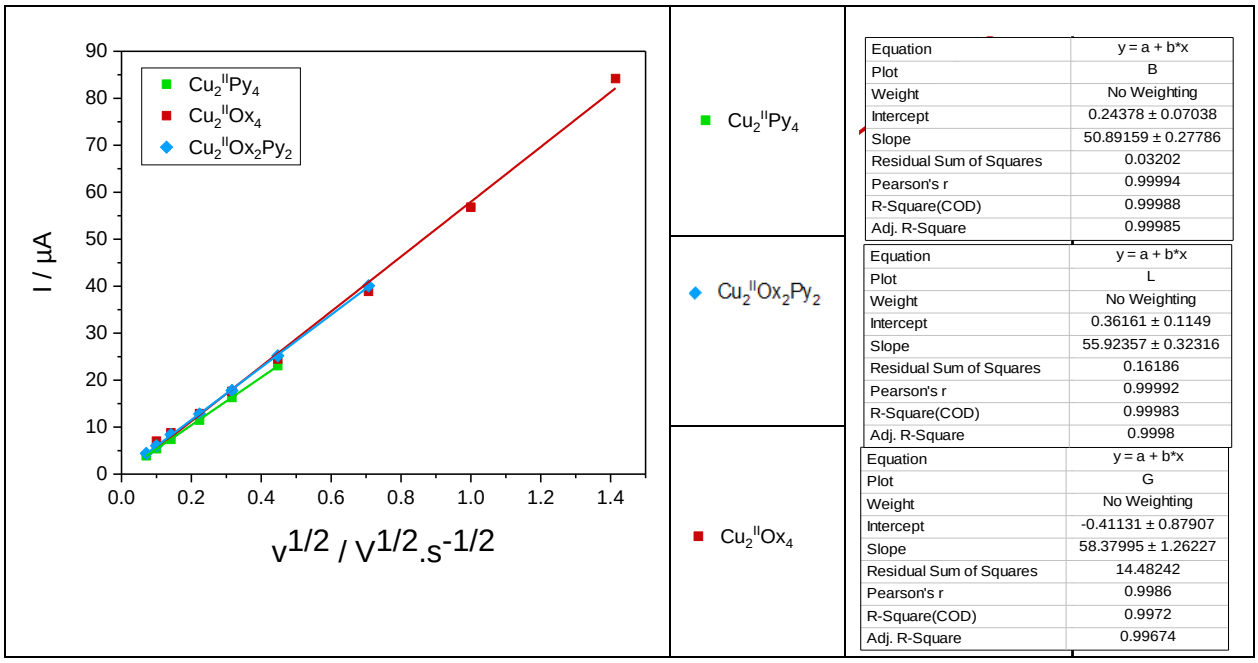

Equation	y = a + b*x
Plot	B
Weight	No Weighting
Intercept	0.24378 ± 0.07038
Slope	50.89159 ± 0.27786
Residual Sum of Squares	0.03202
Pearson's r	0.99994
R-Square(COD)	0.99988
Adj. R-Square	0.99985

Equation	y = a + b*x
Plot	L
Weight	No Weighting
Intercept	0.36161 ± 0.1149
Slope	55.92357 ± 0.32316
Residual Sum of Squares	0.16186
Pearson's r	0.99992
R-Square(COD)	0.99983
Adj. R-Square	0.9998

Equation	y = a + b*x
Plot	G
Weight	No Weighting
Intercept	-0.41131 ± 0.87907
Slope	58.37995 ± 1.26227
Residual Sum of Squares	14.48242
Pearson's r	0.9986
R-Square(COD)	0.9972
Adj. R-Square	0.99674

Figure S10: Plots of the *I* against $v^{1/2}$ for complexes **1**, **2** and $[(Cu_2(Py_4))(\mu\text{-}OH)_2](CF_3SO_3)_2$ for comparison

4-4. EPR spectroscopy

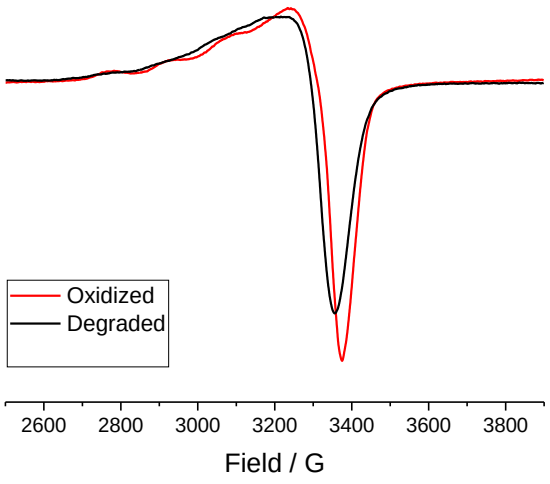

Figure S11: EPR spectrum of the mono-oxidized complex **1** after bulk electrolysis at -40°C, and after heating to room temperature (black). Parameters: frozen solution of 0.7 mM of complex **1** in 0.1 M NBu_4ClO_4 in acetonitrile; T = 15 K; frequency = 9.419 GHz. Simulation was carried out with the EasySpin software© assuming the following parameter: $g_{\perp}$ = 2.070, $g_{//}$ = 2.291, $A_{\perp}$ = 18 G, $A_{//}$ = 177 G.

4-5. UV-Vis-NIR spectroelectrochemistry

Complex **1**

(a)

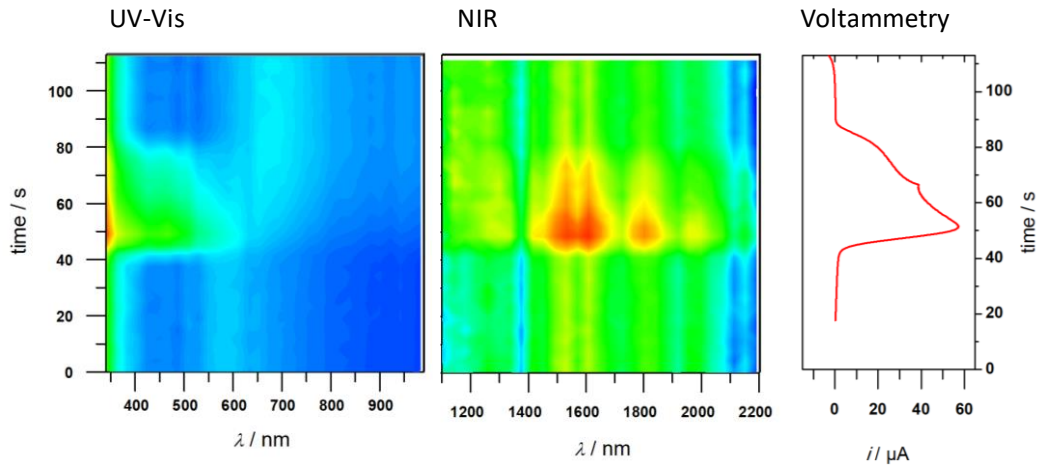

(b)

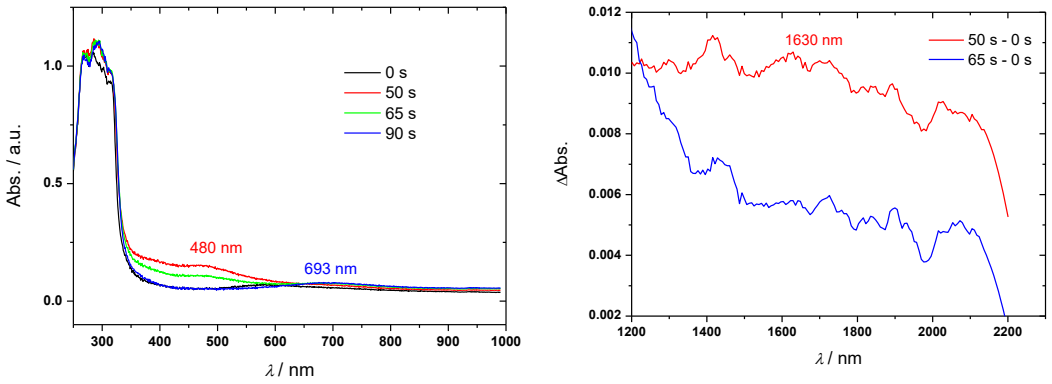

(c)

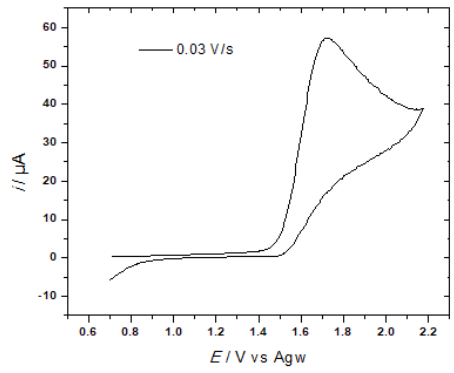

Figure S12: UV-Vis-NIR spectroelectrochemistry data in CH_3CN/NBu_4ClO_4 0.1 M of compound **1** (*C* = 6.8 mM, optical path 0.2 mm, baseline CH_3CN/NBu_4ClO_4 0.1 M) at room temperature; (a) Time-monitoring of the oxidation process (right: current variation with time from CV shown in (c)); (b) Selected UV-Vis (left) and NIR (right) spectra from the spectroelectrochemical monitoring at different time intervals; (c) CV of the complex during the spectroelectrochemical measurement (*v* = 30 mV/s).

Complex **2**

(a)

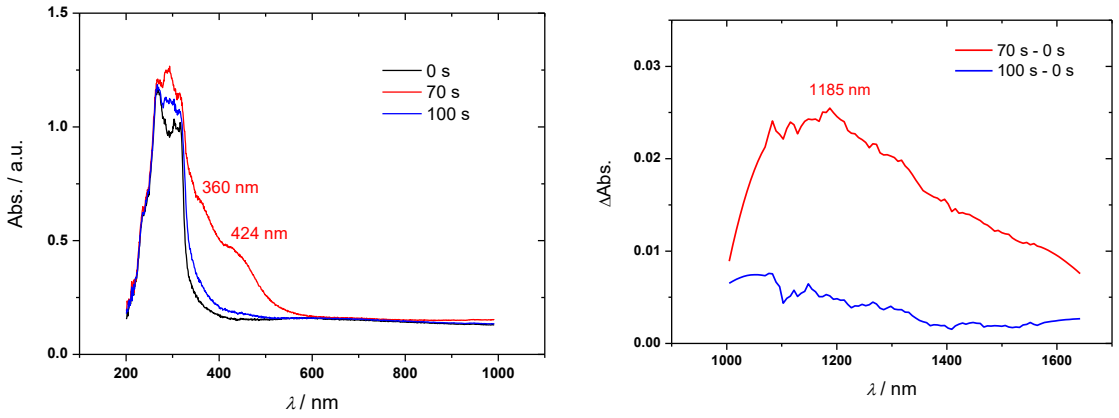

(b)

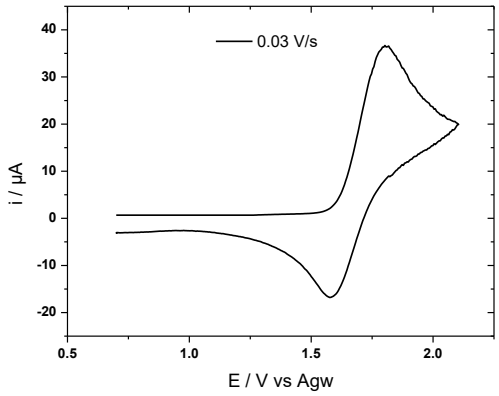

Figure S13: UV-Vis-NIR spectroelectrochemistry data in CH_3CN/NBu_4ClO_4 0.1 M of compound **2** (*C* = 7.0 mM, optical path 0.2 mm, baseline CH_3CN/NBu_4ClO_4 0.1 M) at room temperature; (a) Selected UV-Vis (left) and NIR (right) spectra from the spectroelectrochemical monitoring at different time intervals (see Fig. 5); (b) CV of the complex during the spectroelectrochemical measurement (*v* = 30 mV/s).

4-6. Analysis of the NIR band for complex **2**

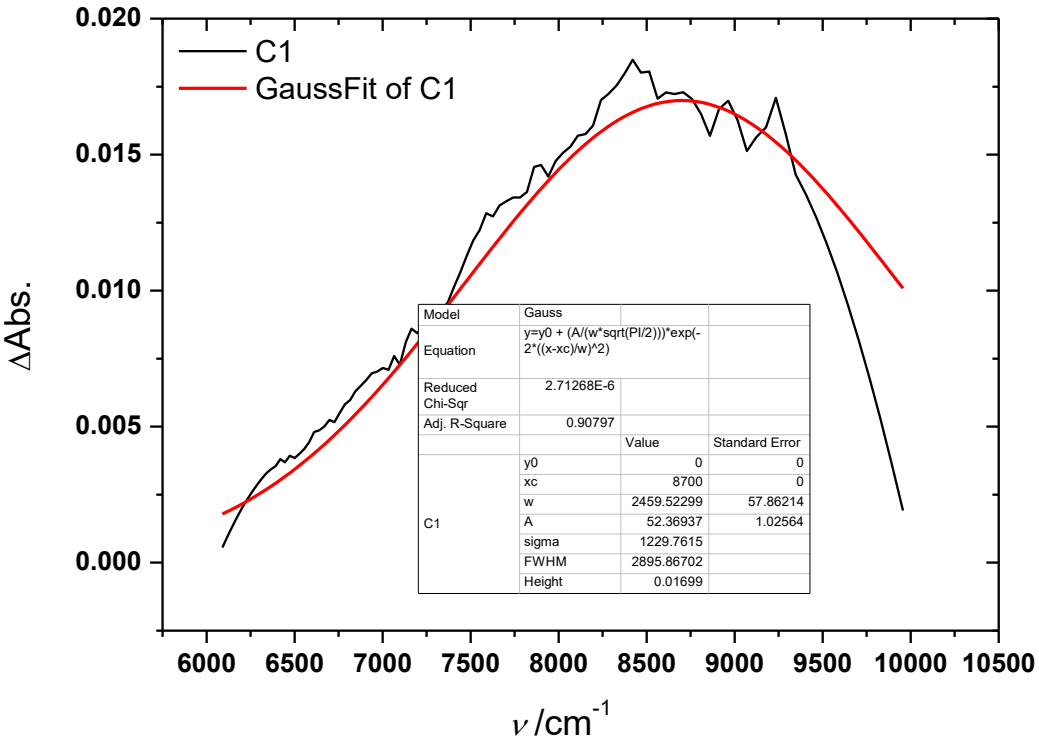

Figure S14: Experimental (black curve) and simulated (red curve, Gaussian shape) of the NIR band obtained by spectroelectrochemistry in CH_3CN/NBu_4ClO_4 0.1 M of compound **2** (*C* = 7.0 mM, optical path 0.2 mm, baseline CH_3CN/NBu_4ClO_4 0.1 M) at room temperature.

The electronic coupling matrix element H_{AB} can be determined from the Mulliken-Hush expression: (references 40 and 41 of the main text)

$$H_{AB} = 0.0206\left(\varepsilon_{max}\breve{\upsilon}_{max}\Delta\breve{\upsilon}_{\frac{1}{2}}\right)^{1/2}/R_{AB}$$

where ε_{max} is the extinction coefficient at the band maximum (120 M^{-1} cm^{-1}), $\breve{\upsilon}_{max}$ the energy at the band maximum (8700 cm^{-1}), $\Delta\breve{\upsilon}_{1/2}$ the bandwidth at half-height (2460 cm^{-1}) and R_{AB} the effective charge transfer distance (2.80 Å). The value found for H_{AB} is 373 cm^{-1}.

The parameter Γ relates to the ratio between the experimental and theoretical values of $\Delta\breve{\upsilon}_{1/2}$:

$$\Gamma = 1 - \frac{(\Delta\breve{\upsilon}_{1/2,exp})}{(\Delta\breve{\upsilon}_{1/2,theo})}$$

For a class II system in the Robin-Day classification, (reference 38 of the main text) $\Delta\breve{\upsilon}_{1/2,theo}$ is given by:

$$\Delta\breve{\upsilon}_{1/2,theo} = (2310\breve{\upsilon}_{max})^{1/2}$$

Hence, for $\breve{\upsilon}_{max}$ = 8700 cm^{-1}, $\Delta\breve{\upsilon}_{1/2,theo}$ = 4125 cm^{-1} and Γ = 0.45 (for class II: 0.1 < Γ < 0.5)

5-Reactivity Studies of Cu^{II}_2 complexes

5-1.ESI-MS after electrolysis and demetallation

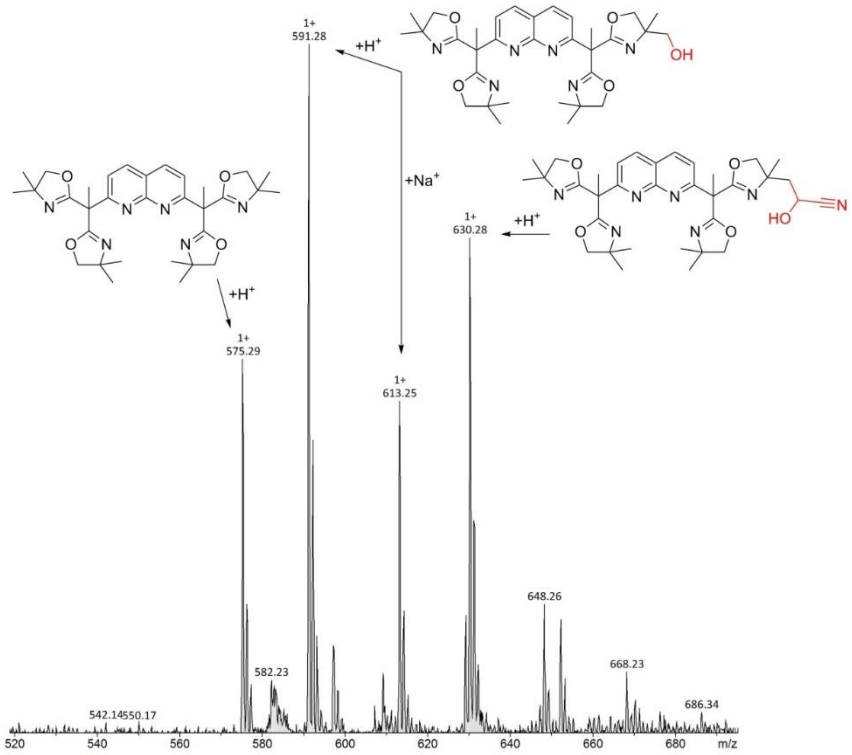

Figure S15: ESI-MS spectrum of the complex $Cu^{II}_2Ox_4$ after electrolysis, demetallation and purification by column chromatography. The initial ligand and possible structures of the oxidized ligand are shown.

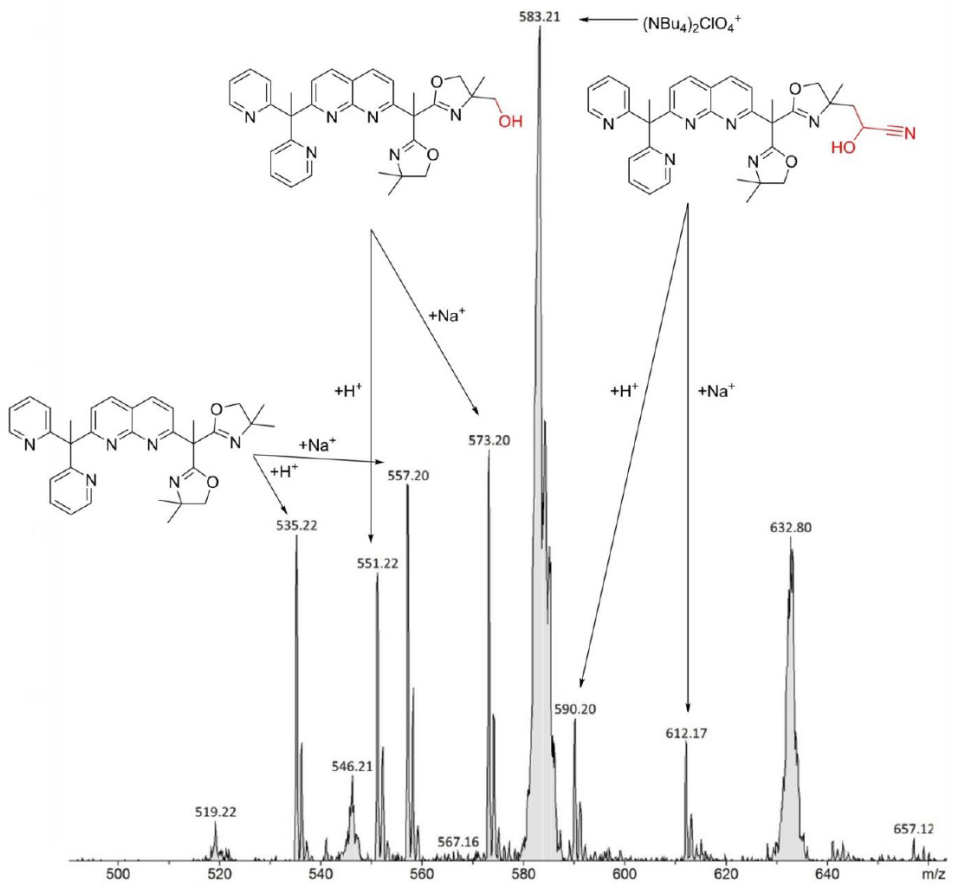

Figure S16: ESI-MS spectrum of the complex $Cu^{II}_2Ox_2Py_2$ after electrolysis, demetallation and purification by column chromatography. The initial ligand and possible structures of the oxidized ligand are shown.

5-2.Proposed mechanisms

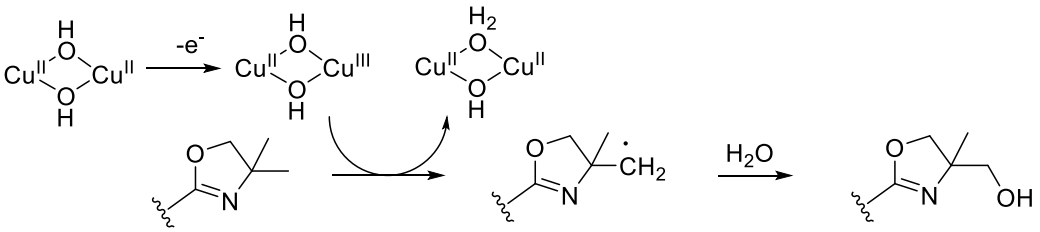

and

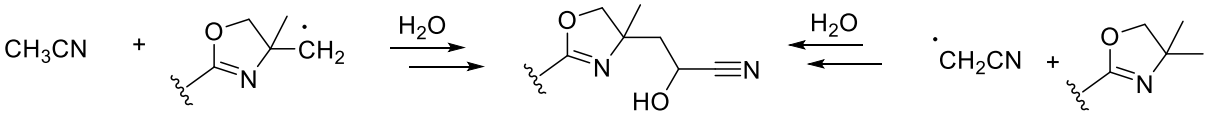

Figure S17: Possible mechanisms for the formation of LOH and LCHOHCN